Phenomenological Arrhenius type constitutive equation for a 304 stainless steel during hot deformation

J. Rasti *[1], A. Najafizadeh [2], S. Jafari [3], B. Khodabandeloo [4]

[1,3,4] Department of Mechanical Engineering, Qom University of Technology (QUT), Qom, Iran
[2] Department of Materials Engineering, Isfahan University of Technology, Isfahan, Iran

Abstract

The present study aimed to present a phenomenological and empirically-based constitutive model to predict the flow behavior of 304 stainless steel. Hot compression tests were performed at temperatures of 950-1100 °C and strain rates of 0.005-0.5 s^{-1} up to the strain of 1. To demonstrate flow curves, three regimes were considered including the linear trend up to yield stress, the work hardening-recovery dominant region based on Estrin and Mecking model from the yield point up to the saturation stress, and the recovery-recrystallization zone from the critical stress extends toward the steady state stress. The Avrami-type equation was supposed for the kinetics of recrystallization and validated by the evolved microstructures at strain 1. Eventually, the six equations that describe the model via strain, strain rate, and temperature were presented. They have included the Arrhenius type equation for the yield, saturation, and steady-state stresses, in addition to the critical strains and the inflection strains together with the relationship for the exponent of Avrami-type recrystallization kinetics formula, all as functions of Zener-Hollomon parameter. Comparing the flow curves predicted by the model with the experimental results showed satisfactory coincidence, confirming that the proposed model can give an almost accurate estimation of the flow stresses of 304 stainless steel at different conditions.

Keywords: Hot deformation; 304 stainless steel; Constitutive equation; Dynamic recrystallization; Arrhenius equation.

1. Introduction

It has been widely confirmed that thermo-mechanical processing is an effective technology to control microstructure and obtain excellent mechanical properties in stainless steels by optimizing the process parameters, such as a measure of strain, temperature, and strain rate. A vast amount of information regarding the relationship between various factors encountered in the hot forming of materials can be expressed in the form of constitutive equations. Constitutive equations can be derived from a macroscopic or microscopic view. Phenomenological equations are derived based on the macroscopic view. This type of modeling establishes the correlation between the measurable parameters such as flow stress, strain, strain rate, and temperature, in the framework of mathematical functions [1, 2].

The most common type of stainless steel in use is grade 304. This grade offers impressive strength, as well as incredible corrosion resistance, lending it to applications in which contact with food, chemicals, or freshwater must be tolerated. Cognitive Market Research has published a market volume of 304 Stainless Steel about 30% of global production of stainless steel (~50 million tons).

Different constitutive equations have been proposed so far by various researchers. Some of these relationships can be seen in Table 1. Since these equations correlate the flow stress with temperature, strain, and strain rate, finding the proper equation and then relevant parameters is a tedious, difficult, and time-consuming task.

**Corresponding author*
Email: rasti@qut.ac.ir
Address: Dep. of Mechanical Engineering,
Qom University of Technology (QUT),
Qom, Zip:1519-37195 Iran
1. Assistant Professor
2. Professor
3. M.Sc. Student
4. M.Sc. Student

Table 1. Different constitutive equations for the modeling of flow curves.

Field Backofen (FB) [1]	$\sigma = K\varepsilon^n\dot{\varepsilon}^m \qquad K = f(T,\dot{\varepsilon}), n = g(T,\dot{\varepsilon}), m = h(T)$
Modified FB [2,3]	$\sigma = K\varepsilon^n\dot{\varepsilon}^m \exp(\mathrm{b}T + \mathrm{s}\varepsilon) \quad n = f(T,\dot{\varepsilon}), m = g(T), K, b, s = \text{const.}$
Johnson Cook (JC) [4]	$\sigma = (A + B\varepsilon^n)\left[1 + C\ln\left(\frac{\dot{\varepsilon}}{\dot{\varepsilon}_0}\right)\right]\left[1 - \left(\frac{T-T_r}{T_m-T_r}\right)^m\right],\ A, B, n, C, \dot{\varepsilon}_0, T_r, T_m$=const.
Modified JC [5]	$\sigma = (A_0 + A_1\varepsilon + A_2\varepsilon^2)\left(1 + D_1\left(\frac{\dot{\varepsilon}}{\dot{\varepsilon}_0}\right)\right)\exp\left[\left(\lambda_1 + \lambda_2\ln\left(\frac{\dot{\varepsilon}}{\dot{\varepsilon}_0}\right)\right)(T - T_r)\right]$ $A_0, A_1, A_2, D_1, \dot{\varepsilon}_0, \lambda_1, \lambda_2, T_r = \text{const.}$
JC with grain size effect [6]	$\sigma = (A + B\varepsilon^n)\left[1 + \lambda\left(\frac{d}{d_0}\right)\right]\left[1 + C_1\ln\left(\frac{\dot{\varepsilon}}{\dot{\varepsilon}_0}\right)\right]\exp\left[\left(f\left(\frac{d}{d_0}\right) + C_1\ln\left(\frac{\dot{\varepsilon}}{\dot{\varepsilon}_0}\right)\right)(T - T_r)\right]$
Arrhenius (Arr) [7-10]	$Z = \dot{\varepsilon}\exp(Q_{\mathrm{def}}/RT) = \begin{cases} B\,\sigma_{\mathrm{P}}{}^{n'} \\ A'\exp(\beta\sigma_{\mathrm{P}}) \\ A\left(\sinh(\alpha\sigma_{\mathrm{P}})\right)^n \end{cases}$ $Q_{\mathrm{def}}, B, n', A', \beta, A, \alpha, n = \text{const. } or\ f(\varepsilon), R = \text{gas const.}$
Zerilli Armstrong (ZA) [11]	$\sigma = c_0 + B_0\varepsilon^n\exp(-\beta_0 T + \beta_1 \mathrm{T}\ln\dot{\varepsilon})$, n=0.5 in original work
Modified ZA [12]	$\sigma = (A_0 + A_1\varepsilon + A_2\varepsilon^2 + A_3\varepsilon^3)\exp\left[-(B_0 + B_1\varepsilon + B_2\varepsilon^2 + B_3\varepsilon^3)(T - T_r) + (C_0 + C_1(T - T_r) + C_2(T - T_r)^2 + C_3(T - T_r)^3)\ln\left(\frac{\dot{\varepsilon}}{\dot{\varepsilon}_0}\right)\right]$
Hansel Spittle (HS) [13]	$\sigma = A\exp(m_1 T)\varepsilon^{m_2}\dot{\varepsilon}^{m_3}\exp(m_4/\varepsilon)(1+\varepsilon)^{m_5 T}\exp(m_6\varepsilon)\dot{\varepsilon}^{m_7 T}T^{m_8}$
Voyiadjis Abed [14]	$\sigma = (c_1 + c_2\varepsilon^{c_3}) + c_4\left[1 - \left[-c_5 T\ln\left(\frac{\dot{\varepsilon}}{\dot{\varepsilon}_0}\right)\right]^{1/q_1}\right]^{1/q_2} + c_6\varepsilon^{c_7}\left[1 - \left[-c_5 T\ln\left(\frac{\dot{\varepsilon}}{\dot{\varepsilon}_0}\right)\right]^{1/q_1}\right]^{1/q_2}$

Among these equations, the sine hyperbolic Arrhenius type equation was used extensively for the modeling of the characteristic stresses as a function of the Zener–Hollomon parameter (*Z*) [7-10, 15, 16].

$$Z = \dot{\varepsilon}\exp(Q_{\mathrm{def}}/RT) = A\left(\sinh(\alpha\sigma)\right)^n \quad \text{or} \quad \text{Eq. (1)}$$

$$\dot{\varepsilon} = A\left(\sinh(\alpha\sigma)\right)^n\exp(-Q_{\mathrm{def}}/RT)$$

Where $\dot{\varepsilon}$ is the strain rate (s^{-1}), A, α, and n are constants independent of temperature, σ is the characteristic stress (MPa), Q_{def} is the hot deformation activation energy (J mol^{-1}), R is the gas constant and T is the absolute temperature (K) of deformation. By mathematical manipulation, the flow stress may be rewritten as a function of *Z* as follows:

$$\sigma = \frac{1}{\alpha}\left\{\left(\frac{Z}{A}\right)^{1/n} + \left[\left(\frac{Z}{A}\right)^{2/n} + 1\right]^{1/2}\right\} \qquad \text{Eq. (2)}$$

Fig. 1a shows schematically the stress-strain curve obtained during the deformation of materials exhibiting the dynamic recrystallization process (DRX). Characteristic stresses, namely the critical stress (σ_{C}) for the initiation of DRX, the peak stress (σ_{P}), the saturation stress (σ_{S}), and the steady state stress (σ_{SS}) can be determined from the strain hardening rate ($\theta = d\sigma/d\varepsilon$) vs flow stress ($\sigma$) plot (Fig. 1b). The critical stress (σ_{C}) and consequently the critical strain for the onset of the DRX can be identified using the Poliak and Jonas method [17-19] modified by Najafizadeh and Jonas [20] as an inflection point of θ-σ plot.

After determining the above characteristic stresses for the different deformation conditions, a constitutive equation such as sine hyperbolic Eqs. (1) or (2) may be used to model them. The procedure for finding proper parameters for this equation is described below.

The graph up to the yield strength(σ_0) has almost a linear trend, afterward, the stress-strain curve can be distinguished by two different domains: 1- the extent from σ_0 to σ_{C} which continues to the saturation stress σ_{S}, where called the work hardening and dynamic recovery (WH) zone, and 2- the extent begins at σ_{C} and continues toward the σ_{P} and finally σ_{SS}, named as dynamically recrystallized zone (DRX).

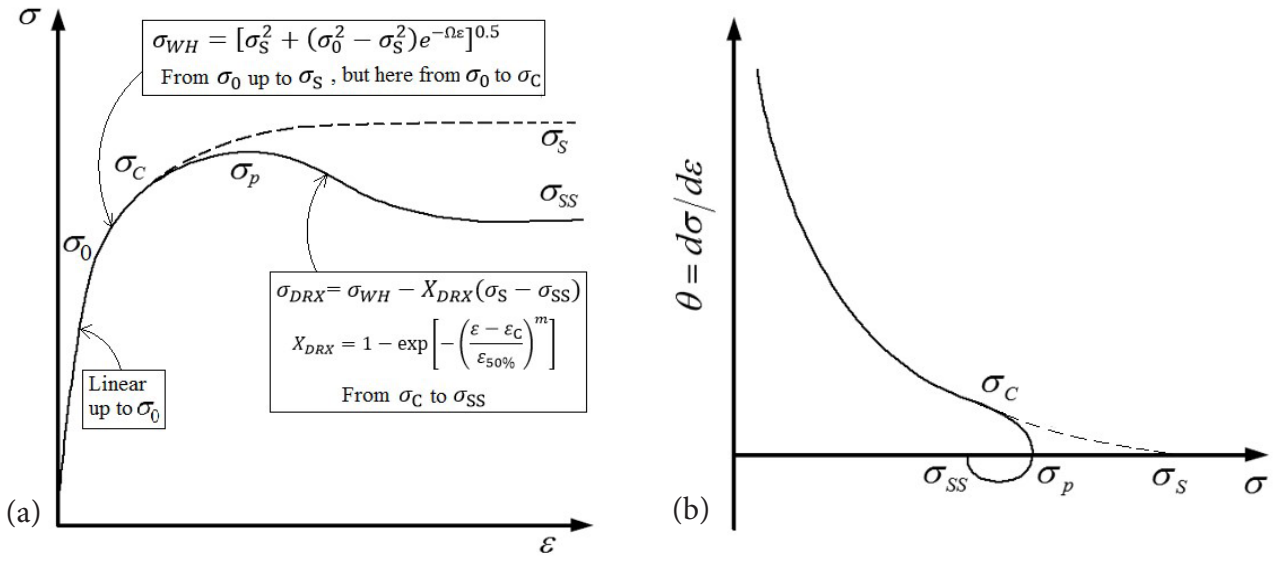

Fig. 1. (a) The schematic flow curve showing the characteristic stresses including the critical stress (σ_C), the peak stress (σ_p), the saturation stress (σ_S), and the steady state stress (σ_{SS}), and (b) the procedure of determining them by drawing the strain hardening rate vs. stress.

1.1. Modeling the work hardening and dynamic recovery (WH) zone

Generally, the Taylor relationship is accepted between the flow stress and dislocation density as $= \sigma_0 + M\alpha Gb\sqrt{\rho}$. The rate of dislocation generated by the plastic work and its rate of removal by dynamic recovery determines the total work hardening:

$$\frac{d\rho}{dt} = \left(\frac{d\rho}{dt}\right)_{\text{Plastic work}} + \left(\frac{d\rho}{dt}\right)_{\text{Recovery}} \quad \text{Eq. (3)}$$

By increasing the dislocation density, the driving force for dynamic recovery is provided. Dynamic recovery reduces that by annihilating positive and negative ones and rearranging them through dislocation climb and cross slip to create sub- or cell-structure (low angle grain boundaries). In austenitic stainless steel due to the low stacking fault energy (about 21 erg/cm^2), this process is not rapid, and hence, with more plastic work, dislocation density severely raises and their distribution is also heterogeneous, which causes the dense cell structure with almost small mean size of $\bar{l}$ (dislocation-free distance) interior grains [21].

Two models for change in dislocation density with strain have been presented. Kock and Mecking (KM) have expressed the following dislocation evolution model [22, 23]:

$$\frac{d\rho}{d\varepsilon} = k_1\sqrt{\rho} - k_2\rho \quad \text{Eq. (4)}$$

Where $k_1\sqrt{\rho}$ is the storage term of mobile dislocations that are locked after distance $\bar{l}$, independent of the temperature, and the second term, $k_2\rho$, relates to the dynamic recovery, which is a function of temperature and strain rates.

Estrin and Mecking (EM) supposed that the dislocation free distance is constant and hence the dislocation accumulation rate is fixed and the equation is rewritten as follows [24].

$$\frac{d\rho}{d\varepsilon} = k - k_2\rho \quad \text{Eq. (5)}$$

Where $k=(bl)^{-1}$. In this model the stress-strain relationship would be as follow on a macroscopic scale;

$$\frac{\sigma^2 - \sigma_S^2}{\sigma_0^2 - \sigma_S^2} = \exp\left(-\frac{\varepsilon}{\varepsilon_C}\right) \quad \text{Eq. (6)}$$

Where ε_C is a specific strain dependent on the material and σ_S is the saturation stress. Robert [25] also reported that at the strains above 0.05, $\theta=d\sigma/d\varepsilon$ has a linear relationship with $1/\sigma$, so the following relationship is established.

$$\theta = \frac{A}{\sigma} - B\sigma \quad \text{Eq. (7)}$$

In this case, the dislocation density changes according to the EM equation: Eq. (8)

$$\frac{d\rho}{d\varepsilon} = U - \Omega\rho \;\rightarrow\; \rho = \rho_0 e^{-\Omega\varepsilon} + (U/\Omega)(1 - e^{-\Omega\varepsilon})$$

And the WH flow stress equation can be expressed below which is the same as Eq. (6):

$$\sigma_{WH} = [\sigma_S^2 + (\sigma_0^2 - \sigma_S^2)e^{-\Omega\varepsilon}]^{0.5} \quad \text{Eq. (9)}$$

1.2. Modeling the DRX region

The flow stress just after the onset of DRX regard-

ing the softening effect of recrystallization phenomena against the work hardening regime with the following assumption:

$$X_{DRX}(\varepsilon) = \frac{\sigma_{WH}(\varepsilon)-\sigma_{DRX}(\varepsilon)}{\sigma_S-\sigma_{SS}}, \quad \text{Eq. (10)}$$

$$\sigma_{DRX} = \sigma_{WH} - X_{DRX}(\sigma_S - \sigma_{SS})$$

Therefore, by knowing the recrystallized fraction at different strains (X_{DRX}), the flow curve beyond the recrystallization onset can be extracted. The recrystallized fraction can be also modeled with the modified Avrami-type equation as follows [26],

$$X_{DRX} = 1 - \exp\left[-\left(\frac{\varepsilon - \varepsilon_C}{\varepsilon_{50\%}}\right)^m\right] \quad \text{Eq. (11)}$$

Where ε_C is the strain for the onset of dynamic recrystallization and $\varepsilon_{50\%}$ is the strain equivalent to the 50% DRX progress (can be regarded as ε^*, the strain at maximum softening rate which is a function of temperature and strain rate [27]) and m is the constant showing the transformation kinetics.

Regarding the literature review, almost articles considering the constitutive equation of 304 stainless steel were based merely on the mathematical manipulation of flow curves via the curve fitting method and did not include phenomenological and microstructural insight. Consequently, this article involved in determining the expressions for the yield stress (σ_0), the saturation stress (σ_S), and the steady state stress (σ_{SS}) as well as the equations for the critical (ε_C) and inflection strains (ε_i) and the exponent of Avrami-type kinetics for the recrystallization (m), the six parameters that the proposed phenomenological model is based on those relations via strain, strain rate, and temperature.

2. Material and Methods

AISI 304 stainless steel with a chemical composition (wt.%) of Fe-0.033% C-9.07% Ni-18.3% Cr-1.97% Mn-0.342% Si-0.573% Mo-0.075% Ti-0.023% P was used in this study. Cylindrical samples 15 mm in height and 10 mm in diameter were machined from the hot rolled bars. The initial grain size of the hot rolled bar was 6 μm, where after annealing at 1100 °C for 30 min, the homogenized microstructure with an average grain size of 40 μm was attained before deformation based on the Heyn intercept method (ASTM E-112). Hot compression tests were carried out in order to study the recrystallization behavior during deformation. Mica plates and BN powder were used for lubricating. The samples were heated by four SiC elements set in the furnace of compression apparatus to the deformation temperatures of 950, 1000, 1050, and 1100 °C and held for 2 min for temperature homogenization. Deformation was carried out at strain rates of 0.005, 0.05, and 0.5 s^{-1} to the true strain of 1, and samples were then quenched immediately (<1 s) after deformation to investigate the DRX microstructures. Samples were then cut along the compression axis and after grinding and polishing, they were etched electrochemically in a 65% nitric acid solution. In order to minimize the effect of friction on the stress-strain curves and correct them, the method of Ebrahimi and Najafizadeh was used [28].

3. Results and Discussion

3.1. Characteristic stresses evaluation

Fig. 2 shows the stress-strain curves obtained from the hot compression tests under various deformation conditions. All the samples exhibited typical DRX flow curves with a single peak stress followed by a gradual fall towards a steady state stress. At the highest strain rate tested (0.5 s^{-1}), a clear delay for the start of DRX can be observed, so the steady state condition is not achieved.

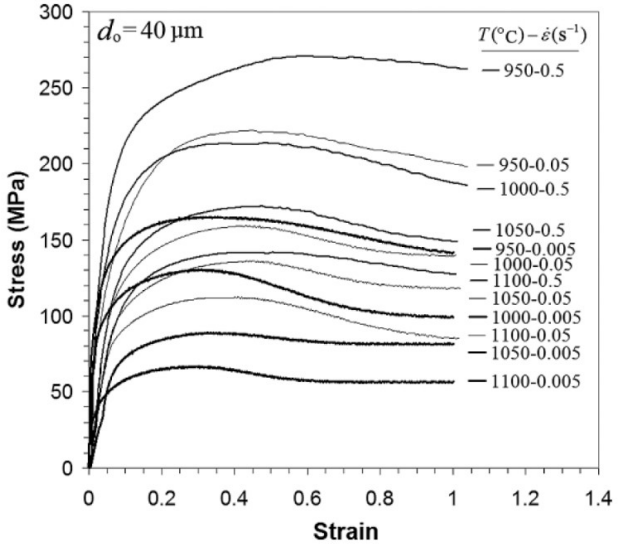

Fig. 2. Stress–strain curves at different deformation temperatures and strain rates.

Eqs. (1) and (2) can be employed for any characteristic stresses including the yield stress (σ_0), the peak stress (σ_P), the saturation stress (σ_S), and the steady state stress (σ_{SS}). Four constant parameters including A, α, n, and Q should be determined for any of these stresses. The procedure will be described as follows for the peak stress, similarly the same trend must be straightforwardly accomplished for the other characteristic stresses aforementioned.

First, Eq. (1) should be rewritten as below:

$$\ln(\dot{\varepsilon}) = \ln A + n\ln[\sinh(\alpha\sigma_P)] - Q_{def}/RT \quad \text{Eq. (12)}$$

With the assumption of α=0.01, the constant n can be determined by the relationship between ln ($\dot{\varepsilon}$) and ln [sinh($\alpha\sigma_P$)] as follows:

$$n = \left.\frac{\partial \ln(\dot{\varepsilon})}{\partial \ln[\sinh(\alpha\sigma_P)]}\right|_{T=const.} \quad \text{Eq. (13)}$$

By assuming that $\alpha\sigma_P$>1.2 the $\sinh(\alpha\sigma_P) \cong \frac{1}{2}\exp(\alpha\sigma_P)$, and therefore the Eq. 12 can be expressed as below,

$$\ln(\dot{\varepsilon}) = \ln A - n\ln(2) + n\alpha\,\sigma_P - Q_{def}/RT \quad \text{Eq. (14)}$$

So, the coefficient $n\alpha$ may be determined by the relationship between ln ($\dot{\varepsilon}$) and σ_P as follows:

$$n\alpha = \left.\frac{\partial \ln(\dot{\varepsilon})}{\partial\,\sigma_P}\right|_{T=const.} \quad \text{Eq. (15)}$$

Hence, by knowing n, the parameter α can be obtained and again employed for determining the constant n at Eq. (4) and this return cycle continues to finally the closely same values for α and n acquired with variation less than 10%. After then, with knowing n and α the activation energy of deformation can be determined by the relationship between ln[sinh($\alpha\sigma_P$)] and $1/T$ as follows:

$$Q_{def} = nR\left.\frac{\partial \ln[\sinh(\alpha\sigma_P)]}{\partial\,(1/T)}\right|_{\dot{\varepsilon}=const.} \quad \text{Eq. (16)}$$

Eventually, the parameter A can be attained from the y-intercept value of straight-line regression of data ln(Z) as the y-axis vs. ln [sinh($\alpha\sigma_P$)] as the x-axis.

Fig. 3 shows the above trends for the peak stress. The following constants were accordingly obtained: A=1.542×10^{19} s^{-1}, n=4.56, α=0.0116, and Q_{def}= 546.7 kJ/mol.

Similarly, the same trends were employed for the other characteristic stresses. The relevant constants were then obtained as can be seen in Table 2.

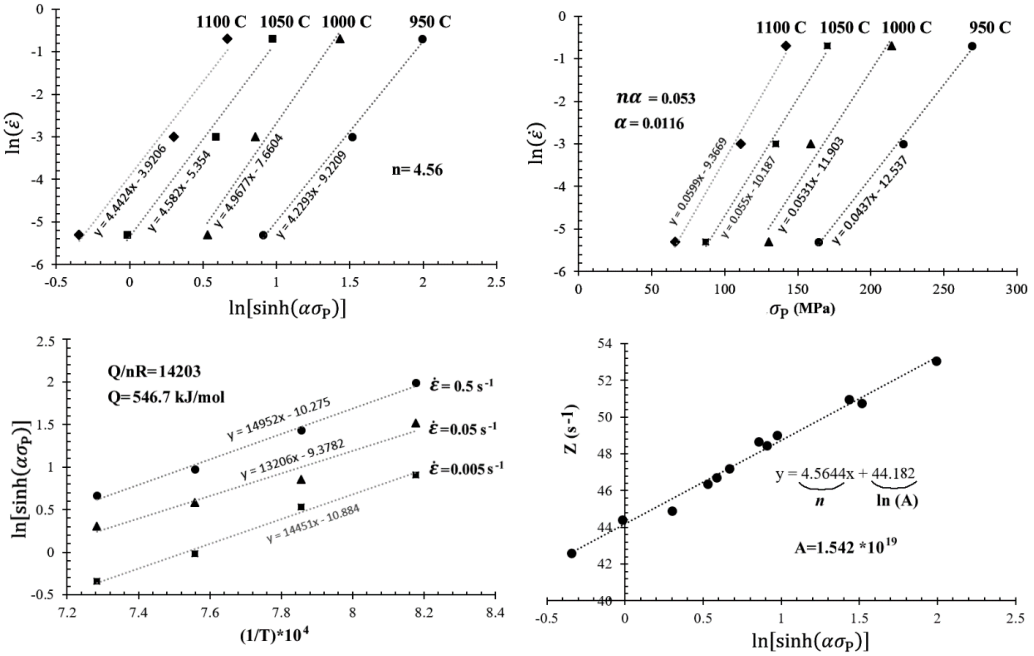

Fig. 3. Determination procedure for the constants of Eq. (1) for the peak stress.

Table 2. The constants of Eq. (1) for the different characteristic stresses.

Stress	A (s^{-1})	n	α (MPa^{-1})	Q_{def} (kJ/mol)
Yield stress (σ_0)	3×10^{21}	6.68	0.01	519
Peak stress (σ_P)	1.542×10^{19}	4.56	0.0116	546.7
Saturation stress (σ_S)	1.15×10^{19}	4.45	0.0099	544
Steady state stress (σ_{SS})	1.6×10^{19}	6.15	0.0052	484

Mohebbi et al. [29] proposed the sine hyperbolic Arrhenius equation for the peak stresses of flow curves of an Nb-Ti micro-alloyed steel considering the self-diffusion activation energy as a dominant mechanism. They proposed a constant value of n=5 based on Cabera et al. work [30] where the deformation process is controlled by the mechanism of dislocation glide and climb. Indeed, in the Nb, Nb-B, and Cu-Nb-B steels, the amount of Q_{def} is very close to its self-diffusion activation energy in the austenite phase, Q_{SD}, but in HSLA steels and austenitic stainless steels, the Q_{def} value is greater than Q_{SD}, due to the impact influence of the precipitations and impurities on the accumulation of dislocations and microstructural changes, even at a very small extent. For example, If instead of σ_p in the above relations σ_{SS} is used, less activation energy is obtained, Q (σ_{SS}) < Q (σ_p) [22]. Long et al. used another approach for modeling of flow curves of a magnesium alloy considering the parameters A, α , n, and Q as a function of temperature and strain rate [31].

3.2. Characteristic strain evaluation

The characteristic strains namely critical strain (ε_C) for the initiation of DRX, the strain corresponding to the peak stress (peak strain = ε_p), the strain equivalent to the inflection point on the stress-strain curve (inflection strain = ε_i), and the strain corresponding to the onset of steady-state flow (steady state strain = ε_{SS}), were also determined in this study (Fig. 4). The critical strain was identified using the Poliak and Jonas method [18] modified by Najafizadeh and Jonas [20]. In their approach, the initiation of DRX is believed to be the inflection point in the strain hardening rate ($\theta=d\sigma/d\varepsilon$) vs flow stress ($\sigma$) plot. The values of ε_i were also identified from the inflection points on the stress-strain curves located between the peak and steady-state stresses. The relation of the critical strain to the peak strain was $\varepsilon_C/\varepsilon_P \cong 0.58$ which is in good accordance with the results of the previous work on 304 steel with an initial grain size of 35 µm ($\varepsilon_C/\varepsilon_p \cong 0.6$) [32] but somewhat lower than that reported by Kim and Yoo [27] for material with an initial grain size of 100 µm ($\varepsilon_C/\varepsilon_p \cong 0.73$).

In all following relationships, the parameter Z was regarded as $Z = \dot{\varepsilon} \exp\left(\frac{546700}{RT}\right)$.

$$\varepsilon_p = 16.9 \times 10^{-3} Z^{0.0676}$$
$$\varepsilon_{crit} = 2.6 \times 10^{-3} Z^{0.094} \cong 0.58\, \varepsilon_p \quad \text{Eq. (17)}$$
$$\varepsilon_i = 7.3 \times 10^{-3} Z^{0.1}$$
$$\varepsilon_{SS} = 3.9 \times 10^{-3} Z^{0.118}$$

3.3. Modeling the stress-strain curve

In this study, it is supposed that the stress against strain linearly goes up until to yield stress σ_0 and the equivalent strain would be about 0.01~0.03. Beyond this region, from σ_0 to σ_C, the work-hardening region (σ_{WH}) exists and the final region from σ_C to σ_{SS} would be the DRX zone (σ_{DRX}). For the initiation of DRX, the critical strain ε_C was used instead of σ_C.

3.3.1. The work hardening and dynamic recovery (WH) zone:

As mentioned earlier, the below equation was used for the modeling of the WH zone:

$$\sigma_{WH}(\varepsilon, \dot{\varepsilon}, T) = [\sigma_S^2 + (\sigma_0^2 - \sigma_S^2) e^{-\Omega\varepsilon}]^{0.5} \quad \text{Eq. (18)}$$

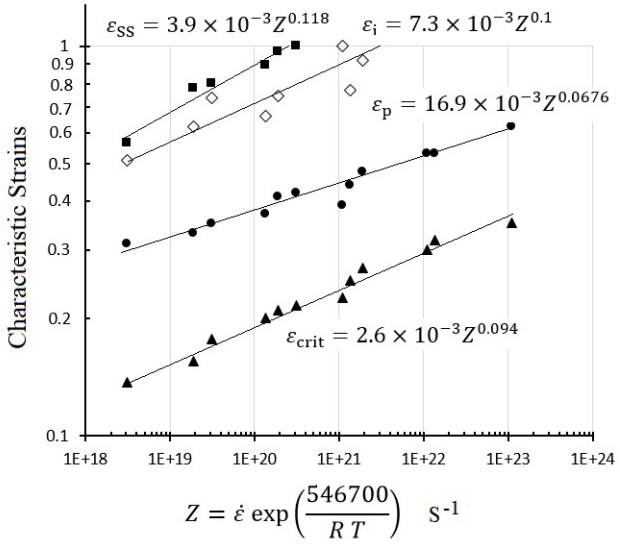

Fig. 4. Characteristic strains of flow curves

In this equation, three parameters including σ_0, σ_S, and Ω were determined. The parameters σ_0 and σ_S are those before expressed in Table 1 as follows:

$$\sigma_0 = \frac{1}{0.01}\left\{\left(\frac{\dot{\varepsilon}\exp(62425/T)}{3\times10^{21}}\right)^{1/6.68} + \left[\left(\frac{\dot{\varepsilon}\exp(62425/T)}{3\times10^{21}}\right)^{2/6.68}+1\right]^{1/2}\right\} \quad \text{Eq. (19)}$$

$$\sigma_S = \frac{1}{0.0099}\left\{\left(\frac{\dot{\varepsilon}\exp(65432/T)}{1.15\times10^{19}}\right)^{1/4.45} + \left[\left(\frac{\dot{\varepsilon}\exp(65432/T)}{1.15\times10^{19}}\right)^{2/4.45}+1\right]^{1/2}\right\} \quad \text{Eq. (20)}$$

The parameter Ω is dependent on the temperature, strain rate, and initial grain size as follows:

$$\Omega = Ad_0^n\dot{\varepsilon}^m exp(Q_\Omega/RT) \quad \text{Eq. (21)}$$

Wahabi et al. [45] have obtained the below equation for Ω in 304H stainless steel regarding Z=ε˙ exp(280,000/RT) which we used accordingly in this model as follows:

$$\Omega = K_\Omega Z^{m_\Omega} = 110\,Z^{-0.096},\ Z = \dot{\varepsilon}\exp(33678/T) \quad \text{Eq. (22)}$$

3.3.2. The DRX zone

Once the applied strain reaches the critical strain for the onset of DRX, ε_C, the following equations should be used together for the modeling of the stress-strain curve.

$$\sigma_{DRX} = \sigma_{WH} - X_{DRX}\times(\sigma_S - \sigma_{SS}) \quad \text{Eq. (23)}$$

$$X_{DRX} = 1 - \exp\left[-\left(\frac{\varepsilon-\varepsilon_C}{\varepsilon_{50\%}}\right)^m\right]$$

Equations of σ_{WH} and σ_S are those expressed before in Eqs. 18 and 20, respectively. The equation of σ_{SS} is that said in Table 1 below.

$$\sigma_{SS} = \frac{1}{0.0052}\left\{\left(\frac{\dot{\varepsilon}\exp(58215/T)}{1.6\times10^{19}}\right)^{1/6.15} + \left[\left(\frac{\dot{\varepsilon}\exp(58215/T)}{1.6\times10^{19}}\right)^{2/6.15}+1\right]^{1/2}\right\} \quad \text{Eq. (24)}$$

The critical strain for the onset of DRX, ε_C may be rewritten as follows:

$$\varepsilon_C = 2.6\times10^{-3}Z^{0.094} = 2.6\times10^{-3}\dot{\varepsilon}^{0.094}\exp(6181/T) \quad \text{Eq. (25)}$$

The parameter $\varepsilon_{50\%}$ which is the strain equivalent to the 50% DRX progress could be determined by regarding the strain of the inflection point in stress-strain curve (ε_i) in which $\varepsilon_{50\%}=k\varepsilon_i$. Because overcoming the DRX causes the curvature of the stress-strain curve to change, therefore the strain $\varepsilon_{50\%}$ must be placed before the strain ε_i. We used then the following equation for the strain $\varepsilon_{50\%}$:

$$\varepsilon_{50\%} = 0.7\varepsilon_i = 5.11\times10^{-3}\dot{\varepsilon}^{0.1}\exp(6576/T) \quad \text{Eq. (26)}$$

It's worth saying that the higher the $\varepsilon_{50\%}$, the greater the width of the concavity portion of the stress-strain curve.

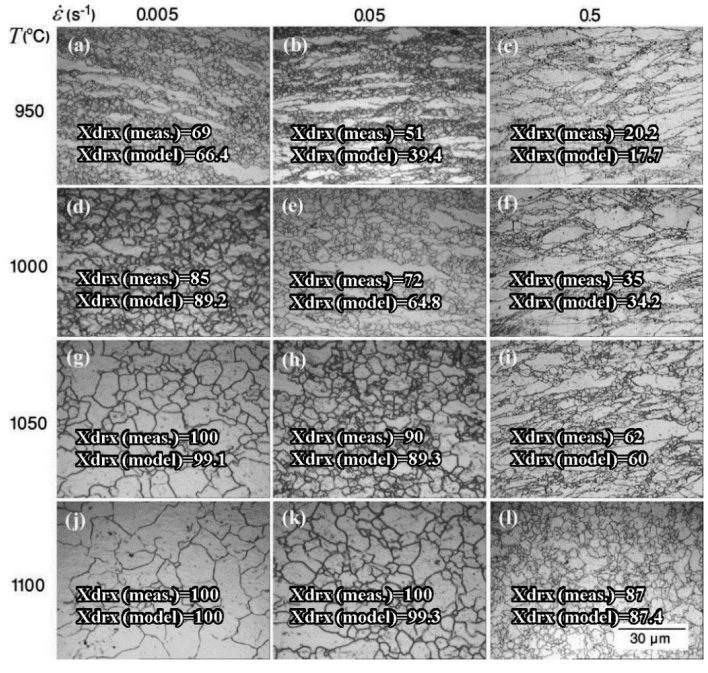

Fig. 5. Microstructures in the quench samples at strain 1 with the evaluated recrystallized fraction (Xdrx (meas.)) compared with the results of model (Xdrx (model)) at different deformation conditions.

Finally, the *m* value which is a constant showing the transformation kinetics could be determined by considering the DRX evolution at strain 1 at different deformation conditions. The following equation was used for the exponent *m*:

$$m = 8.7 \times 10^{-7} \dot{\varepsilon}^{0.03} T^{2.1} \quad \text{Eq. (27)}$$

Fig. 5 shows the microscopic images taken from the quench samples at strain 1 which the recrystallized fractions calculated experimentally as well as those predicted by the model. Fig. 6 implies that there is a good coincidence between the model results and the experimental evidence.

3.3.3. Evaluation of the model

The above equations were used to draw the stress-strain curves at different conditions. Fig. 7 shows the stress-strain curves derived from the model (dotted curve) as compared with the experimental equivalents. There is a satisfactory coincidence between them.

The advantage of the method used in this study for predicting flow curves compared to methods employing four or seven polynomial fittings for A, α, n, and Q, [8,9] is the prediction of microstructure evolution together with the flow curve. Moreover, this model is based on well-known characteristic stresses and strains.

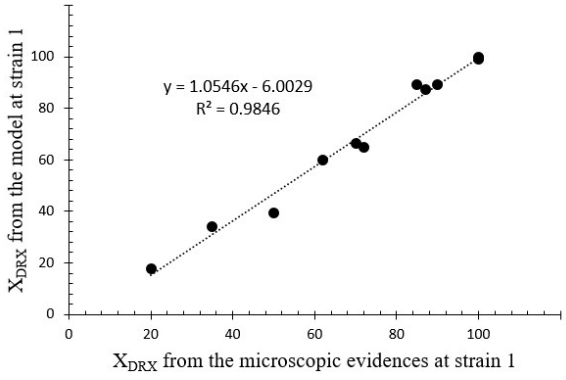

Fig. 6. DRX fraction evaluation from the microstructure against the model results.

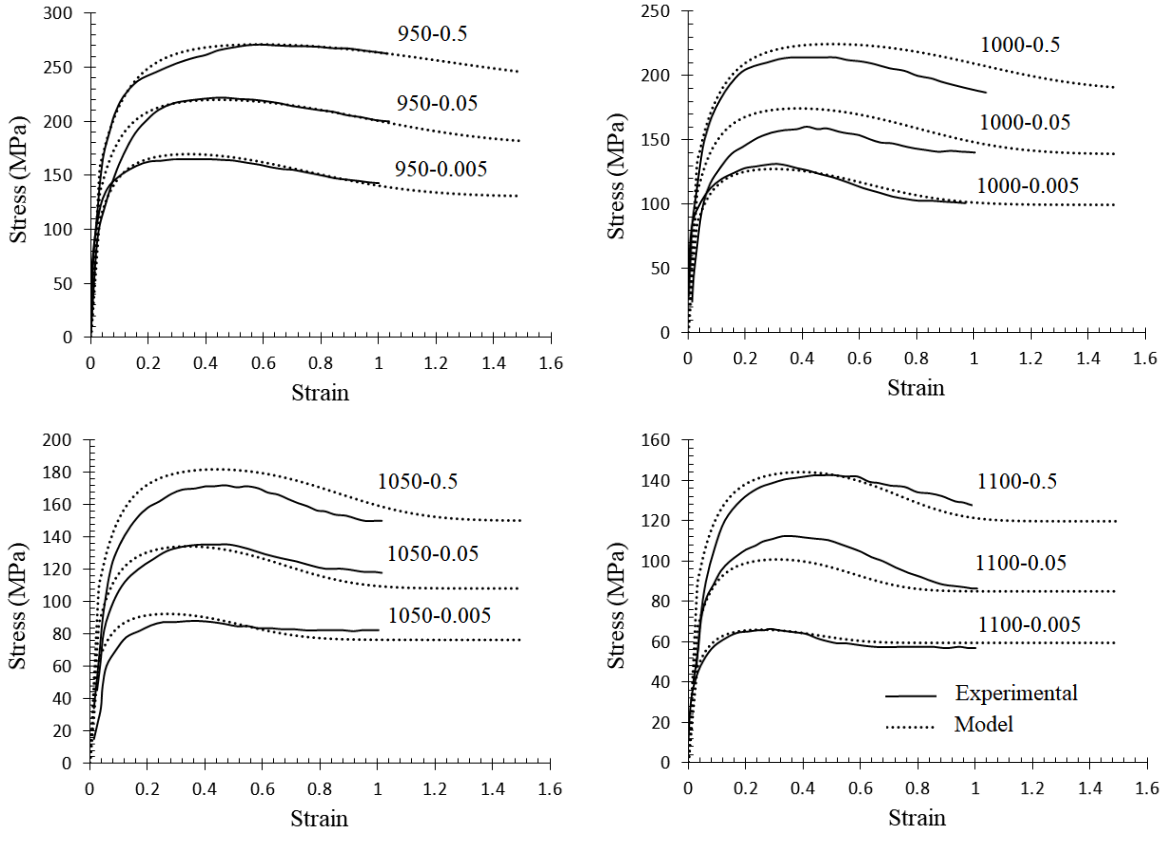

Fig. 7. Stress-Strain curves: Experimental (solid line) against the model results (dotted line).

4. Conclusions

In this study, AISI 304 stainless steel was used in hot compression tests at the temperatures of 950-1100 °C and strain rates of 0.005-0.5 s^{-1} up to the strain of 1. The following results could be extracted:

- The characteristic stresses including yield, critical, peak, saturation, and steady-state stresses were obtained and represented via Zener–Hollomon parameter in an Arrhenius-type equation. Also, the characteristic strains were obtained as well.
- To model flow curves, equations were presented for different regions including the elastic zone up to yield stress, the work-hardening zone from yield to onset of DRX, and the DRX region from initiation point of recrystallization toward steady-state stress.
- By comparison, a satisfactory coincidence was found between the experimental results and flow curves obtained by the proposed model. Moreover, the model could predict well the kinetics of DRX as compared with the experimentally evolved microstructures.

Acknowledgments

The present work has been supported by the vice president of education and research of the Qom University of Technology (QUT).

References

[1] D.S. Fields, W.A. Backofen, Determination of Strain Hardening Characteristics by Torsion Testing, Proceedings-American Society of Testing Materials. 57 (1957) 1259-1272.

[2] K. Nitin, N.K. Hansoge, K.G. Amit, K.S. Swadesh, Study of Hot Deformation Behavior Using Phenomenological Based Constitutive Model for Austenitic Stainless Steel 316, Mater Today: Proceedings. 5 (2018) 4870-4877.

[3] G. Ji, L. Li, F. Qin, L. Zhu, Q. Li, Comparative study of phenomenological constitutive equations for an as-rolled M50NiL steel during hot deformation, J. Alloy Compd. 695 (2017) 2389-2399.

[4] Y.C. Lin, X. Chen, A critical review of experimental results and constitutive descriptions for metals and alloys in hot working, Materials and Design. 32 (2011) 1733-1759.

[5] W.J. Lu, L.Q. Hou, X.Q. Zhang, P.M. Xu, Thermal deformation properties and Johnson-Cook models for superaustenitic stainless steel, J. Plasticity Eng. 23 (2016) 125-130.

[6] H. R. Rezaei Ashtiani, A. A. Shayanpoor, Trans. Nonferrous Met. Soc. China. 31 (2021) 345−357.

[7] Y. Ban, Y. Zhang, Y. Jia, B. Tian, A. A. Volinsky, X. Zhang, Q. Zhang, Y. Geng, Y. Liu, X. Li, Effects of Cr addition on the constitutive equation and precipitated phases of copper alloy during hot deformation. Materials and Design. 191 (2020) 108613.

[8] S. Aliakbari Sani, G.R. Ebrahimi, H. Vafaeenezhad, A.R. Kiani-Rashid, Modeling of hot deformation behavior and prediction of flow stress of a magnesium alloy using constitutive equation and artificial neural network (ANN) model, Journal of Magnesium and Alloys. 6 (2018) 134–144.

[9]H. Wu, J. Yang, F. Zhu, C. Wu, Hot compressive flow stress modeling of homogenized AZ61 Mg alloy using strain-dependent constitutive equations, Materials Science & Engineering A. 574 (2013) 17–24.

[10] Q. Dai, Y. Deng, J. Tang, Y. Wang, Deformation characteristics and strain-compensated constitutive equation for AA5083 aluminum alloy under hot compression, Trans. Nonferrous Met. Soc. China. 29 (2019) 2252−2261.

[11] F.J. Zerilli, R.W. Armstrong, Dislocation-mechanics-based constitutive relations for material dynamics calculations, Journal of Applied Physics. 61 (1987) 1816-1825.

[12] X. Huang, B. Wang, Y. Zang, H. Ji, B. Guan, Y. Li, X. Tang, Constitutive relationships of 21-4 N heat-resistant steel for the hot forging process, J Mater. Res. Technol. 9(6) (2020) 13575–13593

[13] A. Hensel, T. Spittel. Kraft- und Arbeitsbedarf bildsamer Formgebungsverfahren. VEB DeutscherVerlag fur Grundstoffindustrie, Leipzig, 1978, ISBN: 5991fb-6601cdf532e1408fc6566c7635

[14] A. Tabei, F. H. Abed, G. Z. Voyiadjis, H. Garmestani, Constitutive Modeling of Ti-6Al-4V at a Wide Range of Temperatures and Strain Rates, European Journal of Mechanics /A Solids. 63 (2017) 128-135.

[15] C. Zener, H. Hollomon,. Effect of strain-rate upon the plastic flow of steel. J. Appl. Phys. 15 (1944) 22–27.

[16] J.J. Jonas, C.M. Sellars, M.W.J. Tegart, Strength and structure under hot working conditions. Int. Met. Rev. 14 (1969) 1–24.

[17] E.I. Poliak, J.J. Jonas, Initiation of dynamic recrystallization in constant strain rate hot deformation, ISIJ Int. 43(5) (2003) 684-691.

[18] E.I. Poliak, J.J. Jonas, Critical strain for dynamic recrystallization in variable strain rate hot deformation, ISIJ Int. 43(5) (2003) 692-700.

[19] W. Roberts, B. Ahlblom, A nucleation criterion for dynamic recrystallization during hot working, Acta Metall. 26 (1978) 801-813.

[20] A. Najafizadeh, J.J. Jonas, Int. J. ISSI. 3 (2006) 1.

[21]R. Sandstrom, R. Lagneborg, Acta Metall. 23 (1975) 387.

[22]A. Laasraoui, J.J. Jonas, Prediction of steel flow stresses at high temperatures and strain rates, Metall. Trans. A 22A…. (1991) 1545-1558.

[23]W. Wei, K.X. Wei, G.J. Fan, A new constitutive equation for strain hardening and softening of FCC metals during severe plastic deformation, Acta Mater. 56

(2008) 4771–4779.
[24] Y. Estrin, H. Mecking, Acta Mater. 32 (1984) 57.
[25] W. Roberts, Deformation, Processing and Structure, ASM Handbooks, Metals Park, OH, p. 109, 1984.
[26] J.J. Jonas, X. Quelennec, L. Jiang, M. Etienne, The Avrami kinetics of dynamic recrystallization, Acta Mater. (2009) 114-119.
[27] S.I. Kim, Y.C. Yoo, Mater. Sci. Eng. A. 311 (2001) 108.
[28] R. Ebrahimi, A. Najafizadeh, J. Mater. Proc. Tech. 152 (2004) 136.
[29] M.S. Mohebbi, M.H. Parsa, M. Rezayat, Analysis of Flow Behavior of an Nb-Ti Microalloyed Steel During Hot Deformation, Metall Mater Trans A. 49 (2018) 1604–1614. https://doi.org/10.1007/s11661-018-4536-0
[30] J.M. Cabrera, A. Al Omar,J.M. Prado, Modeling the flow behavior of a medium carbon microalloyed steel under hot working conditions, Metall Mater Trans A. 28 (1997) 2233–2244. https://doi.org/10.1007/s11661-997-0181-8
[31] J. Long, Q. Xia, G. Xiao, Y. Qin, S. Yuan, Flow characterization of magnesium alloy ZK61 during hot deformation with improved constitutive equations and using activation energy maps. Inter. J. Mech. Sci. 191 (2021) 1060-69.
[32] A. Dehghan-Manshadi, P.D. Hodgson, Metall. Mater. Trans. A 39 (2008) 28-30.